Journal of Materials Chemistry A

COMMUNICATION

View Article Online
View Journal | View Issue

Cite this: J. Mater. Chem. A, 2019, 7, 2490

Received 26th November 2018
Accepted 17th December 2018

DOI: 10.1039/c8ta11383a

rsc.li/materials-a

Emulsion polymerization derived organic photocatalysts for improved light-driven hydrogen evolution†

Catherine M. Aitchison, Reiner Sebastian Sprick * and Andrew I. Cooper *

Here, we present the use of mini-emulsion polymerization to generate small particle analogues of three insoluble conjugated polymer photocatalysts. These materials show hydrogen evolution rates with a sacrificial donor under broadband illumination that are between two and three times higher than the corresponding bulk polymers. The most active emulsion particles displayed a hydrogen evolution rate of 60.6 mmol h^{-1} g^{-1} under visible light ($\lambda > 420$ nm), which is the highest reported rate for an organic polymer. More importantly, the emulsion particles display far better catalytic lifetimes than previous polymer nanoparticles and they are also effective at high concentrations, allowing external quantum efficiencies as high as 20.4% at 420 nm. A limited degree of aggregation of the polymer particles maximizes the photocatalytic activity, possibly because of light scattering and enhanced light absorption.

Semiconductor photocatalysts that produce hydrogen directly from water are a potential technology for renewable, carbon-free energy generation. Poly(*p*-phenylene) was shown to be active for photocatalytic proton reduction in 1985,[1] but inorganic materials have since dominated this area.[2,3] However, there has been a renewed interest in organic materials for solar fuel production since the first report of the photocatalytic activity of carbon nitride in 2009.[4] Organic materials such as polymers have molecular structures that can be tailored by synthesis, and this allows for tuning of optoelectronic and physical properties.[5] An expanding variety of polymeric materials have been developed for photocatalytic hydrogen production including (i) covalent triazine-based frameworks (CTFs);[6,7] (ii) covalent organic frameworks (COFs) with imine,[8] hydrazone[9] and azine linkages;[10] (iii) linear conjugated polymers,[11–13] and; (iv) conjugated microporous polymers (CMPs)[5,12,14,15] In the presence of a sacrificial electron donor, quantum efficiencies up to 50% at 420 nm have been demonstrated.[16] Organic materials have also been reported to catalyze overall water splitting, both as composites with carbon[17,18] and, recently, as single-phase polymeric photocatalysts.[19]

In addition to developing materials with different chemical structures, performance can also be improved by optimizing the morphology of the photocatalysts. For example, structuring of metal oxide semiconductors has produced a variety of nanomorphologies that have improved photocatalytic performance compared to bulk materials.[20] Techniques such as hydrolysis[21] and stabilizer controlled precipitation[22] have been used to synthesize nanoparticles of suspension photocatalysts, while chemical vapor deposition[23,24] and solution growth[25] are commonly used in the fabrication of nanostructured films and photoelectrodes. Recently, there have also been reports of morphology modification of organic photocatalysts by nanocasting,[26–28] soft templating[29,30] and solvothermal methods.[31,32]

One approach to tailoring the morphology of organic photocatalysts is to prepare alkylated, solution-processable, conjugated polymers, which can be processed after synthesis into thin films[33] or nanoparticles.[34,35] In particular, conjugated polymer nanoparticles based on dialkyl-fluorene-co-benzothiadiazole polymers were reported to give very high initial hydrogen evolutions rates (HERs) of up to 50 mmol g^{-1} h^{-1}.[34,36] The high initial HERs for the nanoparticles are, presumably, a result of the surface-to-volume ratio of the nanoparticles, which were prepared by anti-solvent precipitation to give particle diameters in the range 20–100 nm.[34] Unfortunately, though, these materials showed poor long-term colloidal stability as compared to non-alkylated insoluble bulk polymers, which have more modest HERs rates but much greater catalytic stability.[11,12]

Most heterogeneous organic photocatalysts are obtained by precipitation polymerization, mainly as insoluble solids, in the form of relatively large particles (2–100 μm). Hence, there are potential advantages in developing methods to reduce particle size in these materials while maintaining colloidal stability in the photocatalytic reaction medium.

Exciton diffusion lengths in conjugated polymers are typically around 5–20 nm:[37–39] as such, a large proportion of

Department of Chemistry and Materials Innovation Factory, 51 Oxford Street, Liverpool, L7 3NY, UK. E-mail: ssprick@liverpool.ac.uk; aicooper@liverpool.ac.uk

† Electronic supplementary information (ESI) available. See DOI: 10.1039/c8ta11383a

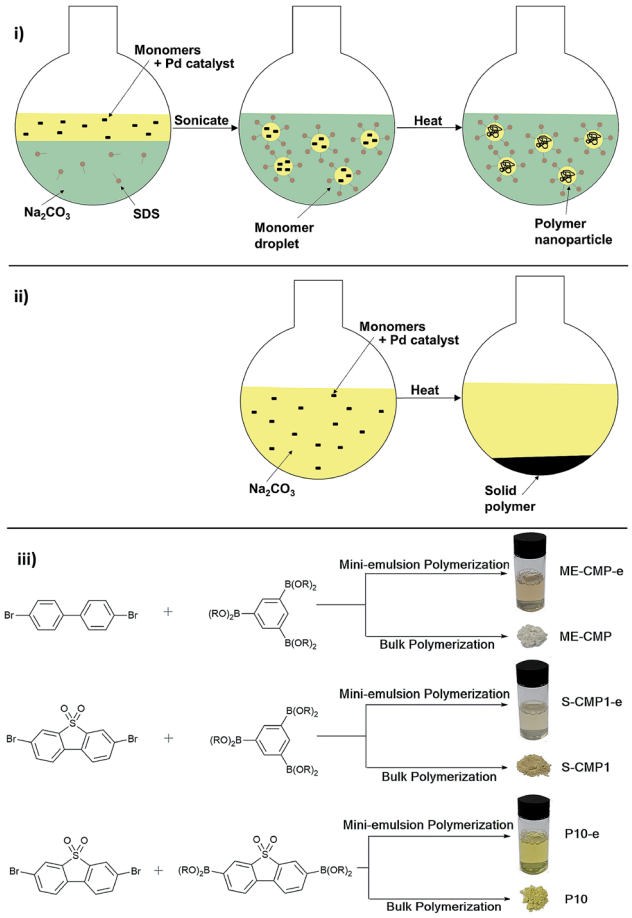

Fig. 1 (i) Mini-emulsion polymerization. (ii) Bulk precipitation polymerization. (iii) Synthesis route for the six polymers.

photogenerated excitons would be expected to be unable to reach the particle surface for reaction in a bulk polymer catalyst.

Previously, mini-emulsion polymerization has been used to make nanoparticles of otherwise unprocessable linear polymers and CMPs using various coupling chemistries.[40–44] Here, we prepare polymer photocatalysts by mini-emulsion polymerization (Fig. 1(i)) and compared their photocatalytic activity with their bulk counterparts, as synthesized by precipitation polymerization (Fig. 1(ii)). Three systems were explored: a non-alkylated 1,3,5-linked benzene CMP (ME-CMP-e; Fig. 1),[45] a 1,3,5-linked benzene dibenzo[*b*,*d*]thiophene sulfone CMP (S-CMP1-e),[46] and a linear conjugated homopolymer of dibenzo[*b*,*d*]thiophene sulfone (P10-e).[47] This new synthesis route led to photocatalysts with much higher photocatalytic activity than bulk materials. These photocatalysts are also much longer lived than previous conjugated polymer nanoparticle dispersions, which rapidly destabilize.[34,36]

Results and discussion

Bulk polymers ME-CMP, S-CMP1 and P10 were prepared from the respective bromoaryl and aryl diboronic acid ester monomers by Pd(0)-catalyzed Suzuki–Miyaura coupling in DMF/water at 150 °C in the presence of K_2CO_3 (Fig. 1). Nanoparticle analogues of the three bulk polymers (ME-CMP-e, S-CMP1-e and P10-e) were synthesized in mini-emulsions;[43] in all cases, the monomers and $[Pd(PPh_3)_4]$ were dissolved in toluene, followed by addition of an aqueous solution of sodium *n*-dodecyl sulfate (SDS) and Na_2CO_3. The reaction mixture was then sonicated for 2 minutes to give mini-emulsions of toluene droplets stabilized by SDS in water. These mini-emulsions were then heated overnight at 90 °C, cooled to room temperature, and then filtered to remove any aggregated material. The resulting filtrate was a dispersion of the polymer emulsion particles.

Dynamic light scattering (DLS) measurements for the particles obtained by mini-emulsion polymerization showed no material larger than 1 μm in size, with average hydrodynamic diameters (*Z*-average) of 248 nm, 180 nm and 156 nm for ME-CMP-e S-CMP1-e and P10-e, respectively (Fig. S1†). The CMP particles, ME-CMP-e and S-CMP1-e, showed no signs of aggregation over 11 days without stirring, with minimal changes in average particle diameter or size polydispersity as measured by DLS (Fig. S2†). By contrast, the linear P10-e particles flocculated over 9 days to give an average diameter of 400 nm. When sonicated, these 400 nm aggregates could be redispersed and a hydrodynamic radius of 169 nm was found by DLS, close to the original size of the particles directly after synthesis. Scanning electron microscopy (SEM) of the emulsion particles as synthesized showed morphologies that agreed well with the DLS measurements, showing particle sizes from 50 nm up to 500 nm. ME-CMP-e and S-CMP1 showed a more elongated, tendril-like morphology compared to P10-e, which comprised roughly spherical particles (Fig. 2A–C). Increasing sonication time during synthesis was found to have no effect on particle size. A batch of P10-e sonicated for a total of 30 minutes had an average hydrodynamic radius of 161 nm, almost identical to the batch sonicated for 2 minutes (156 nm) (Fig. S3†). This finding is consistent with previous studies of conjugated polymers synthesized in mini-emulsion which showed small particles of approximately 20 nm formed immediately after sonication but that upon heating this coalesce into larger (*ca.* 200 nm) nanostructures.[43]

UV-visible spectroscopy (Fig. 3) revealed differences between the absorption profiles for the CMP emulsion particles and their bulk analogues. Bulk ME-CMP has an absorption onset of 404 nm while in ME-CMP-e, this is shifted further into the UV (358 nm). Similarly, bulk S-CMP1 has absorption onset of 439 nm *versus* 409 nm for S-CMP1-e. It is possible that the lower temperature of the emulsion polymerization resulted in a reduced degree of polycondensation compared to the bulk synthesis at higher temperature. Lower molecular weights have been observed previously for CMPs that were prepared in non-polar solvents such as toluene at lower temperatures, as compared to the same CMP synthesized in aprotic polar solvents, such as DMF, at higher temperatures.[48]

The linear polymers P10 and P10-e showed a smaller difference between their absorption profiles with onsets of 481 nm and 466 nm, respectively. For linear systems, it has been shown previously that low molecular weight oligomers can have similar absorption on-sets compared to the respective polymer.[33]

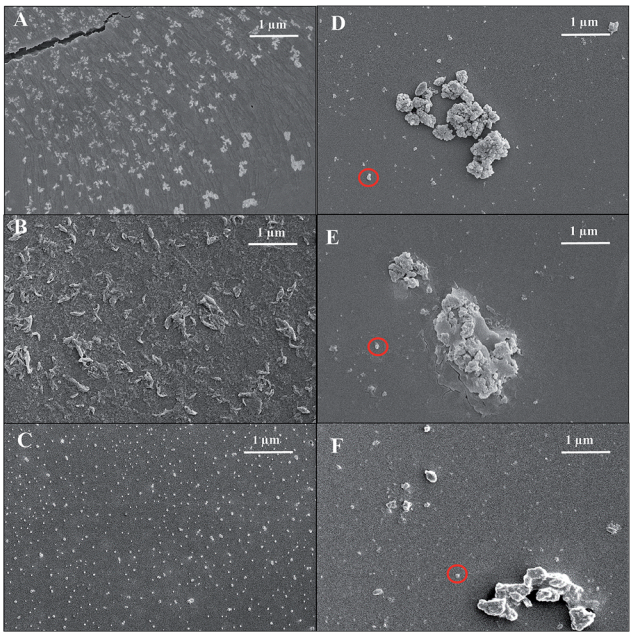

Fig. 2 SEM images of ME-CMP-e (A), S-CMP1-e (B) and P10-e (C) as synthesized and of ME-CMP-e (D), S-CMP1-e (E) and P10-e (F) when collected from the photolysis mixture.

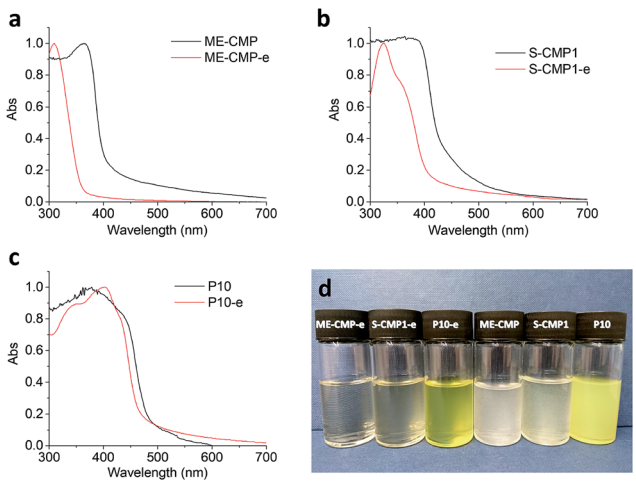

Fig. 3 UV-visible spectra of ME-CMP-e and corresponding bulk polymer, ME-CMP (a), S-CMP1-e and bulk S-CMP1 (b), P10-e and bulk P10 (c), photograph of the nanoparticles or bulk particle in water/methanol/triethylamine (1 : 1 : 1) photolysis mixtures (d); from left to right: ME-CMP-e, S-CMP1-e, P10-e, ME-CMP, S-CMP1, P10 (polymer concentrations are given in Table 1).

It is possible, therefore, that differences in chain length between the linear polymers P10 and P10-e have a more limited effect on the absorption on-set as compared to the two CMPs. The insoluble nature of the polymers meant full analysis of chain length was not possible.

Photocatalytic hydrogen evolution experiments were performed using the emulsion-derived materials as synthesized, because removal of the SDS surfactant by dialysis resulted in flocculation. Dispersions of the bulk polymers were prepared to match those produced during the emulsion polymerization synthesis. That is, these bulk polymer dispersions also contained the water : toluene (9 : 1) mixture, SDS and Na_2CO_3, to be consistent with the emulsion polymers. Both types of dispersions—the emulsion polymers and the bulk analogues—were then added to methanol and triethylamine (TEA) in a 1 : 1 : 1 mixture. In general, the aqueous dispersions prepared from materials produced by emulsion polymerization were less turbid than those of their bulk counterparts (Fig. 3d). As in previous studies, TEA was used as the sacrificial hole-scavenger combined with methanol to aid miscibility with water and also to promote dispersion of these hydrophobic polymers in water. Although no additional metal co-catalyst was added to the photolysis mixtures, residual palladium from the polymerization reaction could be detected in all materials by inductively coupled plasma atomic emission spectroscopy after work up (ESI). Palladium has been shown to play a role in the catalytic cycle[49] but palladium contents of 0.542, 0.420 and 0.403 wt% were measured for ME-CMP-e, S-CMP1-e and P10-e, which are similar to the levels of Pd found in the bulk polymers at 0.363, 0.332 and 0.650 wt%, respectively (Table S4†). These values are also lower than used in the polymerization, indicating some Pd had been removed by filtration during work-up.

All of the nanoparticles produced by miniemulsion polymerization were active under broadband irradiation ($\lambda > 295$ nm), with hydrogen evolution rates of 4.1, 8.1 and 29.5 mmol h^{-1} g^{-1} for ME-CMP-e, S-CMP1-e and P10-e, respectively, significantly outperforming their bulk analogues under the same conditions, with addition of the same concentration of SDS surfactant to the bulk samples for consistency (Table 1). These measurements show that processing these polymers into nanoparticle form can lead to an enhancement in the HER under broadband irradiation conditions by a factor of between two and three. Under visible light irradiation ($\lambda > 420$ nm), ME-CMP-e showed a similar (low) HER as compared to ME-CMP (0.046 *vs.* 0.052 mmol h^{-1} g^{-1}), while S-CMP1-e performed less well than the bulk polymer, S-CMP1 (1.84 *vs.* 2.59 mmol h^{-1} g^{-1}).

This poorer performance under visible light, in contrast to the broadband experiments, can be explained by the blue-shift in the absorption on-set for the two nanoparticle materials (Fig. 3a and b), which appears to offset or outweigh the increased surface area.

In contrast to the two CMPs, both linear polymers, P10-e and P10, absorb a more significant proportion of visible light ($\lambda >$ 420 nm; Fig. 3c), resulting in a HER of 6.13 mmol h^{-1} g^{-1} for the P10 bulk material and a very high HER of 14.52 mmol h^{-1} g^{-1} for P10-e. Repeat experiments with two additional, separate batches of P10-e showed good reproducibility, with HERs of 14.06 and 14.42 mmol h^{-1} g^{-1} under visible light ($\lambda > 420$ nm), respectively. Hydrogen evolution experiments under broadband illumination ($\lambda > 295$ nm) were also performed for three different batches of both ME-CMP-e and S-CMP1-e. The hydrogen evolution rates varied slightly between batches (Fig. S32 and S33†), but all were significantly higher than the bulk polymers.

P10-e was also tested at equivalent concentration to polymer dot photocatalysts reported in the literature[34–36] (13 μg mL^{-1})

Table 1 Hydrogen Evolution Rates (HER) of emulsion polymerized particles compared to bulk polymers

Polymer	Optical gap (eV)	Polymer concentration (mg mL^{-1})	HER[a] λ > 295 nm (mmol h^{-1} g^{-1})	HER[a] λ > 420 nm (mmol h^{-1} g^{-1})
ME-CMP	3.07	0.06	1.72 ± 0.04	0.046 ± 0.002
ME-CMP-e	3.46	0.06	4.40 ± 0.25	0.052 ± 0.001
S-CMP1	2.82	0.07	5.92 ± 0.18	2.59 ± 0.07
S-CMP1-e	3.03	0.07	8.54 ± 0.11	1.84 ± 0.01
P10	2.58	0.1	9.54 ± 0.26	6.13 ± 0.22
P10-e	2.66	0.1	29.46 ± 0.38	14.52 ± 0.31
P10-e	2.66	0.013	—	60.6 ± 1.3

[a] HER determined with catalyst in 25 mL aqueous/methanol/triethylamine 1 : 1 : 1 (aqueous phase containing water : toluene 9 : 1, SDS surfactant 10 mg mL^{-1} and Na_2CO_3 3.5 mg mL^{-1}) irradiated by 300 W Xe light source for 5 hours using a suitable filter. HERs are quoted as the average over 5 hours.

resulting in an increased hydrogen production rate of 60.6 mmol h^{-1} g^{-1} over 5 hours (Fig. 4 and S37†). To our knowledge, this is the highest hydrogen evolution rate reported for any polymer photocatalyst, as normalized to the polymer mass, although we note that a low total amount of hydrogen is produced at such low catalyst concentrations, and hence other metrics, such as external quantum efficiency (discussed below), are a more useful measure of catalyst efficacy. As with other polymeric photocatalysts[4,7,12] we found that the activity of P10-e could be further improved from 60.6 to 84.0 mmol h^{-1} g^{-1} by *in situ* photodeposition of 3 wt% Pt from K_2PtCl_6 onto the material (Fig. S39†). TEM imaging showed the Pt formed 1–10 nm sized particles on the surface of P10-e (Fig. S22†).

Control experiments with P10-e in water without TEA or MeOH produced negligible hydrogen after 6 hours of irradiation as did a control of the mini-emulsion synthesis liquor (water, toluene, Na_2CO_3 and SDS) mixed with TEA and MeOH but without polymer (Fig. S38†). Also, experiments in the dark produced no detectable amount of hydrogen over 5 hours of stirring in water/methanol/TEA (Fig. S38†). Irradiated samples all produced significantly more hydrogen than was present in the polymers themselves (Fig. 4, S34 and S35†). These experiments indicate that the hydrogen production is indeed photocatalytic.

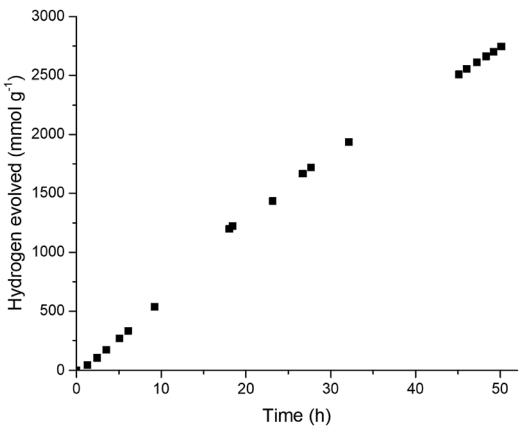

Fig. 4 Hydrogen evolution experiments of P10-e (13 μg mL^{-1}). 325 μg P10-e in 25 mL aqueous/methanol/triethylamine (1 : 1 : 1; aqueous phase containing water : toluene (99 : 1), SDS surfactant 1.3 mg mL^{-1} and Na_2CO_3 0.5 mg mL^{-1}). Irradiated by a 300 W Xe light source fitted with a λ > 420 nm filter. Mixture was degassed by N_2 bubbling after 9, 23, 32 and 45 hours.

Long-term photocatalytic stability is a significant question for organic photocatalysts, especially for the small number nanoparticle systems that have been reported so far. For example, the most active organic photocatalyst to date base on mass-normalized HER[36] (initial rate 50 mmol h^{-1} g^{-1}) was reported to be active for less than 4 hours before total loss of photocatalytic activity. By contrast, ME-CMP-e (the least stable of the materials tested here) showed a reduction in photocatalytic activity after 5 hours under broadband illumination (λ > 295 nm), but the material was still active when the experiment was stopped after 35 hours (Fig. S36†). S-CMP1-e had improved longevity under broadband illumination (λ > 295 nm) compared to ME-CMP-e, with a 46% drop in activity after 20 hours. Significant quantities of hydrogen were still being produced when experiments were stopped after 50 hours (Fig. S36†). Under visible irradiation (λ > 420 nm filter), P10-e produced hydrogen for at least 50 hours, albeit with some reduction from the initial rate (Fig. S37†), and a HER of 7.34 mmol g^{-1} h^{-1} was recorded over the last 5 hours of the experiment. At the lower catalysts concentration (13 μg mL^{-1}) the retention in activity of P10-e was better still, after 50 hours of visible light irradiation the activity had dropped by less than 23% (rate of first five hours was 60.6 mmol h^{-1} g^{-1} *versus* 47.2 mmol h^{-1} g^{-1} for last five hours) (Fig. 4). As such, the stability of these materials is improved greatly over polymer nanoparticle catalysts that have been reported previously.[36]

The external quantum efficiency (EQE) of P10-e (0.1 mg mL^{-1}) at 420 nm was estimated to be 5.8 ± 0.2%, while bulk P10 was 2.3 ± 0.1% under equivalent conditions. These values are lower than those previously reported for P10 (ref. 47) due to a lower concentration of the photo-catalyst. These EQE measurements were performed in a quartz cuvette with a path length of 1 cm and it was noted that, for the optically clear nanoparticle dispersions (Fig. 3d), a significant proportion of the incoming light passed unabsorbed through the sample. By using the same nanoparticle concentration but a path length of 2 cm, the EQE of P10-e increased to 10.5 ± 1.0%. A 5 cm path length gave a value of 14.2 ± 0.2%. As Kisch has noted,[50] comparisons in the saturated regime of catalyst concentration

are particularly useful measures of activity. Here, the EQE could be increased further by increasing the nanoparticle concentration, leading to an optimized value of 20.4 ± 0.4% for P10-e using a 5 cm path length and a nanoparticle concentration of 1 mg mL^{-1}.

Post-photocatalysis DLS measurements of the mini-emulsion materials revealed an increase in particle size, with material over a micron present in all samples. Control experiments (Fig. S4–S6†) revealed that some aggregation occurs within minutes of adding the particle solution to TEA and MeOH; that is, aggregation is caused by the medium, rather than the photolysis. For example, the average particle size of S-CMP1-e in water increased from 180 nm to 1937 nm within 2 minutes of adding methanol/TEA.

Static light scattering measurements of the photolysis mixtures containing the photocatalyst in water/methanol/TEA were used to compare the particle size of the aggregated emulsion particles to those of the bulk polymers (Table 2).

Although the emulsion particles had increased in size compared to the as-made samples, they were still smaller than the corresponding bulk polymer particles. Bulk ME-CMP had particle sizes ranging from 2–100 μm while the aggregated ME-CMP-e emulsion particles were 1–40 μm. Perhaps more significantly, the surface area weighted Sauter mean diameter,[51,52] $D[3,2]$ (see eqn (1) in ESI†), decreased from 16.6 μm for the bulk polymer ME-CMP to 7.94 μm compared to the ME-CMP-e emulsion particles. Likewise, bulk S-CMP1 ranged from 1 μm to over 100 μm with $D[3,2]$ of 20.7 μm, while the emulsion particles, S-CMP1-e, had a maximum size of 20 μm with some sub-micron material also present, giving a smaller $D[3,2]$ of 3.69 μm. The P10 materials gave more multi modal SLS plots: both the bulk and the emulsion nanoparticles showed particles ranging between 1–100 μm along with a smaller fraction between 100–1000 nm in size, but the emulsion system showed a more significant nanoscale fraction ranging from 30 nm to 500 nm. This resulted in a lower $D[3,2]$ value of 0.37 μm for P10-e compared to 2.06 μm for bulk P10 and meant that the relative surface area of the particle size distribution was over five times higher for P10-e (16 390 m^2 kg^{-1}) than for the bulk (2911 m^2 kg^{-1}). The particle size distributions for ME-CMP-e and S-CMP1-e gave relative surface areas of 756 and 1625 m^2 kg^{-1} respectively which were also higher than their bulk analogues (361 and 290 m^2 kg^{-1}).

Particle sizes were also analyzed by SEM. Samples of the emulsion particles collected from the photolysis mixture appeared to contain a polydisperse mixture of aggregates along with 'free' nanoparticles. ME-CMP-e, S-CMP1-e and P10-e (Fig. 2D–F) all contained some material that had aggregate into micron scale particles, but smaller 50 nm to 1 μm particles were still present in all three polymers. We note that the particle size in the low concentration 13 μg mL^{-1} sample of P10-e shows a similarly polydisperse distribution of particle sizes to the sample at 0.1 mg mL^{-1} with a similar $D[3,2]$ of 0.41 (*vs.* 0.37 for 0.1 mg mL^{-1}, see Fig. S12†) we therefore suggest the increase in per gram normalized HER is not a function of aggregation behavior but due to the experiments being in the saturated regime of a concentration-activity graph as discussed by Kisch.[50]

The emulsion particles were also tested for photocatalysis using an alternative sacrificial electron donor (0.1 M ascorbic acid).[53] All three emulsion particle materials were stable to aggregation in this case (Fig. S8†), with particle sizes between 150 and 250 nm (Table S2†) but, contrary to expectation, decreased photocatalytic performances were observed with respect to bulk polymer analogues (Table S3†). For example, un-aggregated P10-e had a rate of 2.01 mmol g^{-1} h^{-1} using ascorbic acid as a donor, while the bulk P10 maintained a higher rate of 4.53 mmol g^{-1} h^{-1}. This effect was observed to an even greater extent when using triethanolamine (TeOA) as the sacrificial donor. In 10 vol% TeOA, we observed colloidally stable dispersion where the apparent hydrodynamic diameters for the emulsion polymers are reduced to 94.3 nm for ME-CMPe, 87.6 nm for S-CMP1-e and 59.0 nm for P10-e (Fig. S7†), but again the smaller emulsion particles gave lower hydrogen evolution rates (Table S3†). For example, the rate of P10-e in TEA/MeOH was 14.52 mmol g^{-1} h^{-1} under visible light (λ > 420 nm) but with 10% TeOA, this was reduced to 0.50 mmol g^{-1} h^{-1}, while the bulk polymer maintained a high rate of 6.83 mmol g^{-1} h^{-1} in TeOA.

These observations suggest that some degree of aggregation might be beneficial for optimal photocatalytic activity of polymers synthesized in mini-emulsion. Materials have been observed before where an increase in particle size is needed to achieve significant photocatalytic activity.[34] Aggregate formation in conjugated polymers has also been linked to improved charge-transport properties.[54]

To investigate this further, NaCl was added to a sample of P10-e in 10% TeOA to induce aggregation. Salt addition led to

Table 2 Particle size under photocatalytic conditions and palladium contents of the polymers

Polymer	$D[3,2]^{a,b}$ (μm)	Relative surface area[a,c] (m^2 kg^{-1})	Pd content[d] (wt%)
ME-CMP	16.6	361	0.363 ± 0.006
ME-CMP-e	7.94	756	0.542 ± 0.002
S-CMP1	20.7	290	0.332 ± 0.007
S-CMP1-e	3.69	1625	0.420 ± 0.003
P10	2.06	2911	0.650 ± 0.020
P10-e	0.37	16 390	0.403 ± 0.001

[a] Bulk and emulsion particle sizes as measured by static light scattering on a Mastersizer 3000 under catalytic conditions, aqueous/methanol/triethylamine 1 : 1 : 1 (aqueous phase containing water : toluene 9 : 1, SDS surfactant 10 mg mL^{-1} and Na_2CO_3 3.5 mg mL^{-1}). [b] Sauter mean diameter (see eqn (1) in ESI). [c] Relative surface area calculated from the total particle surface area divided by total particle weight assuming a density of 1 g cm^{-3}. [d] Palladium content measured by ICP-OES for emulsion samples and ICP-MS for bulk, see ESI for full details.

a particle size increase from 59 nm to 4 μm (Fig. S45†), and the hydrogen evolution rate more than doubled to 1223 μmol h^{-1} g^{-1} for the sample after salt addition (Fig. S46†). The ionic content of water has been shown to play an important role in photocatalytic hydrogen production for carbon nitride,[55] but control reactions for the P10 bulk material with and without NaCl showed almost no variation in HER (Fig. S46†). This suggests that the improvement in HER after salt addition to P10-e is indeed aggregation induced.

We hypothesized that the use of TeOA as a donor (and to a lesser extent ascorbic acid) caused some phase separation between water and residual toluene to occur. This might cause the polymer particles to have limited contact with water and sacrificial hole scavenger. To test this, the residual toluene was removed by centrifugation and P10-e was redispersed in a 10% TeOA solution. The particles were a similar size (59 and 66 nm) before and after toluene removal (Fig. S48†) but the HER increased by a factor of 14, up to 6.94 mmol h^{-1} g^{-1} (Fig. S48†), indicating the importance of the interface between P10-e, water, and the sacrificial electron donor. We noted, however, that the rate was still lower than for aggregated P10-e in a TEA/MeOH/water system, suggesting that the smaller particle size in TeOA was a limiting factor. To mimic this particle aggregation, the toluene-free P10-e material was deposited onto silica colloids. The resultant material was highly polydisperse, with particle sizes ranging from 300 nm to over 100 μm (Fig. S49†). P10-e on the silica support gave a hydrogen evolution of 9.01 mmol h^{-1} g^{-1} in 10% TeOA (Fig. S50†). A control reaction of silica colloids in 10% TeOA produced no hydrogen upon irradiation (Fig. S50†). We believe that the increase in HER that occurs upon deposition onto the silica support is primarily due to light scattering. In this case, improved light capture seems to outweigh any reduction in the active surface area of the catalyst due to aggregation.

Conclusions

In summary, mini-emulsion polymerization was used to create nanoparticulate analogues of photocatalytic polymers with significantly improved catalytic activity. All of the nanomaterials showed greater hydrogen evolution rates from water and a sacrificial TEA/MeOH donor under broad spectrum irradiation than the corresponding bulk materials. In addition, P10-e showed a very high visible light activity of 14.5 mmol h^{-1} g^{-1} along with greatly improved stability compared to the first publications of photocatalytic active P-dots for hydrogen production,[34,36] as well as more recent cycloplatinated examples.[35] Some degree of aggregation of the emulsion particles appears to be beneficial for optimal photocatalytic activity and the best-performing catalysts were mixtures of free nanoparticles and larger aggregates. This may, in part, be related to light absorption mechanisms and scattering effects. Mini-emulsion polymerization allows for the processing of otherwise insoluble and hard-to-process polymeric catalysts. It also opens up potential routes for depositing or incorporating photocatalytic particles into multicomponent composites, for example to construct hybrid systems for overall water splitting in the absence of sacrificial agents. This mini-emulsion route may also be applicable to the production of catalysts for other important reactions, such as CO_2 reduction.

Conflicts of interest

There are no conflicts to declare.

Acknowledgements

We thank the Engineering and Physical Sciences Research Council (EPSRC) for financial support under Grant EP/N004884/1, CMA thanks the EPSRC for financial support through a DTP grant. We thank Dr M. A. Zwijnenburg, Dr T. McDonald, and Dr J. Whittaker for helpful discussions.

Notes and references

1 S. Yanagida, A. Kabumoto, K. Mizumoto, C. Pac and K. J. Yoshinob, *J. Chem. Soc., Chem. Commun.*, 1985, 474–475.
2 T. Jafari, E. Moharreri, A. Amin, R. Miao, W. Song and S. Suib, *Molecules*, 2016, **21**, 900.
3 X. Chen, S. Shen, L. Guo and S. S. Mao, *Chem. Rev.*, 2010, **110**, 6503–6570.
4 X. Wang, K. Maeda, A. Thomas, K. Takanabe, G. Xin, J. M. Carlsson, K. Domen and M. Antonietti, *Nat. Mater.*, 2009, **8**, 76–80.
5 R. S. Sprick, J. X. Jiang, B. Bonillo, S. Ren, T. Ratvijitvech, P. Guiglion, M. A. Zwijnenburg, D. J. Adams and A. I. Cooper, *J. Am. Chem. Soc.*, 2015, **137**, 3265–3270.
6 K. Schwinghammer, S. Hug, M. B. Mesch, J. Senker and B. V. Lotsch, *Energy Environ. Sci.*, 2015, **8**, 3345–3353.
7 J. Bi, W. Fang, L. Li, J. Wang, S. Liang, Y. He, M. Liu and L. Wu, *Macromol. Rapid Commun.*, 2015, **36**, 1799–1805.
8 M. G. Schwab, M. Hamburger, X. Feng, J. Shu, H. W. Spiess, X. Wang, M. Antonietti and K. Müllen, *Chem. Commun.*, 2010, **46**, 8932.
9 L. Stegbauer, K. Schwinghammer and B. V. Lotsch, *Chem. Sci.*, 2014, **5**, 2789–2793.
10 V. S. Vyas, F. Haase, L. Stegbauer, G. Savasci, F. Podjaski, C. Ochsenfeld and B. V. Lotsch, *Nat. Commun.*, 2015, **6**, 8508.
11 R. S. Sprick, B. Bonillo, R. Clowes, P. Guiglion, N. J. Brownbill, B. J. Slater, F. Blanc, M. A. Zwijnenburg, D. J. Adams and A. I. Cooper, *Angew. Chem., Int. Ed.*, 2016, **55**, 1792–1796.
12 C. Yang, B. C. Ma, L. Zhang, S. Lin, S. Ghasimi, K. Landfester, K. A. I. Zhang and X. Wang, *Angew. Chem., Int. Ed.*, 2016, **55**, 9202–9206.
13 X. Zong, X. Miao, S. Hua, L. An, X. Gao, W. Jiang, D. Qu, Z. Zhou, X. Liu and Z. Sun, *Appl. Catal., B*, 2017, **211**, 98–105.
14 K. Kailasam, J. Schmidt, H. Bildirir, G. Zhang, S. Blechert, X. Wang and A. Thomas, *Macromol. Rapid Commun.*, 2013, **34**, 1008–1013.
15 L. Li, W. Y. Lo, Z. Cai, N. Zhang and L. Yu, *Macromolecules*, 2016, **49**, 6903–6909.

16 G. Zhang, G. Li, Z.-A. Lan, L. Lin, A. Savateev, T. Heil, S. Zafeiratos, X. Wang and M. Antonietti, *Angew. Chem., Int. Ed.*, 2017, **56**, 13445–13449.
17 J. Liu, Y. Liu, N. Liu, Y. Han, X. Zhang, H. Huang, Y. Lifshitz, S.-T. Lee, J. Zhong and Z. Kang, *Science*, 2015, **347**, 970–974.
18 W. Che, W. Cheng, T. Yao, F. Tang, W. Liu, H. Su, Y. Huang, Q. Liu, J. Liu, F. Hu, Z. Pan, Z. Sun and S. Wei, *J. Am. Chem. Soc.*, 2017, **139**, 3021–3026.
19 L. Wang, Y. Wan, Y. Ding, S. Wu, Y. Zhang, X. Zhang, G. Zhang, Y. Xiong, X. Wu, J. Yang and H. Xu, *Adv. Mater.*, 2017, **29**, 1702428.
20 F. E. Osterloh, *Chem. Soc. Rev.*, 2013, **42**, 2294–2320.
21 J. Kiwi and M. Gratzel, *J. Chem. Soc., Faraday Trans. 1*, 1987, **83**, 1101–1108.
22 L. Jing, S. V. Kershaw, Y. Li, X. Huang, Y. Li, A. L. Rogach and M. Gao, *Chem. Rev.*, 2016, **116**, 10623–10730.
23 A. Kay, I. Cesar and M. Grätzel, *J. Am. Chem. Soc.*, 2006, **128**, 15714–15721.
24 R. Van de Krol, Y. Liang and J. Schoonman, *J. Mater. Chem.*, 2008, **18**, 2311.
25 J. Y. Kim, G. Magesh, D. H. Youn, J. W. Jang, J. Kubota, K. Domen and J. S. Lee, *Sci. Rep.*, 2013, **3**, 2681.
26 X. Wang, K. Maeda, X. Chen, K. Takanabe, K. Domen, Y. Hou, X. Fu and M. Antonietti, *J. Am. Chem. Soc.*, 2009, **131**, 1680–1681.
27 W. Huang, Z. J. Wang, B. C. Ma, S. Ghasimi, D. Gehrig, E. Laquai, K. Landfester and K. A. I. Zhang, *J. Mater. Chem. A*, 2016, **20**, 7555–7559.
28 K. Zhang, D. Kopetzki, P. H. Seeberger, M. Antonietti and F. Vilela, *Angew. Chem., Int. Ed.*, 2013, **52**, 1432–1436.
29 H. Yan, *Chem. Commun.*, 2012, **48**, 3430–3432.
30 M. F. Ibad, H. Kosslick, J. W. Tomm, M. Frank and A. Schulz, *Microporous Mesoporous Mater.*, 2017, **254**, 136–145.
31 Y. Cui, Y. Tang and X. Wang, *Mater. Lett.*, 2015, **161**, 197–200.
32 X. Lu, L. Gai, D. Cui, Q. Wang, X. Zhao and X. Tao, *Mater. Lett.*, 2007, **61**, 4255–4258.
33 D. Woods, R. S. Sprick, C. L. Smith, A. J. Cowan and A. I. Cooper, *Adv. Energy Mater.*, 2017, **7**, 1700479.
34 L. Wang, R. Fernández-Terán, L. Zhang, D. L. A. Fernandes, L. Tian, H. Chen and H. Tian, *Angew. Chem., Int. Ed.*, 2016, **55**, 12306–12310.
35 P. J. Tseng, C. L. Chang, Y. H. Chan, L. Y. Ting, P. Y. Chen, C. H. Liao, M. L. Tsai and H. H. Chou, *ACS Catal.*, 2018, **8**, 7766–7772.
36 P. B. Pati, G. Damas, L. Tian, D. L. A. Fernandes, L. Zhang, I. B. Pehlivan, T. Edvinsson, C. M. Araujo and H. Tian, *Energy Environ. Sci.*, 2017, **10**, 1372–1376.
37 A. Bruno, L. X. Reynolds, C. Dyer-Smith, J. Nelson and S. A. Haque, *J. Phys. Chem. C*, 2013, **117**, 19832–19838.
38 J. E. Kroeze, T. J. Savenije, M. J. W. Vermeulen and J. M. Warman, *J. Phys. Chem. B*, 2003, **107**, 7696–7705.
39 P. E. Shaw, A. Ruseckas and I. D. W. Samuel, *Adv. Mater.*, 2008, **20**, 3516–3520.
40 M. C. Baier, J. Huber and S. Mecking, *J. Am. Chem. Soc.*, 2009, **131**, 14267–14273.
41 Z. Hashim, P. Howes and M. Green, *J. Mater. Chem.*, 2011, **21**, 1797–1803.
42 K. Wu, J. Guo and C. Wang, *Chem. Commun.*, 2014, **50**, 695–697.
43 B. C. Ma, S. Ghasimi, K. Landfester, F. Vilela and K. A. I. Zhang, *J. Mater. Chem. A*, 2015, **3**, 16064–16071.
44 K. Landfester, *Angew. Chem., Int. Ed.*, 2009, **48**, 4488–4507.
45 R. S. Sprick, B. Bonillo, M. Sachs, R. Clowes, J. R. Durrant, D. J. Adams and A. I. Cooper, *Chem. Commun.*, 2016, **52**, 10008–10011.
46 R. S. Sprick, Y. Bai, A. Y. Guilbert, M. Zbiri, C. M. Aitchison, L. Wilbraham, Y. Yong, D. J. Woods, M. A. Zwijnenburg and A. I. Cooper, *Chem. Mater.*, DOI: 10.1021/acs.chemmater.8b02833.
47 M. Sachs, R. S. Sprick, D. Pearce, S. J. Hillman, A. Monti, A. A. Y. Guilbert, N. J. Brownbill, S. Dimitrov, F. Blanc, M. A. Zwijnenburg, J. Nelson, J. R. Durrant and A. I. Cooper, *Nat. Commun.*, 2018, **9**, 4968.
48 R. Dawson, A. Laybourn, Y. Z. Khimyak, D. J. Adams and A. I. Cooper, *Macromolecules*, 2010, **43**, 8524–8530.
49 L. Li, Z. Cai, Q. Wu, W. Y. Lo, N. Zhang, L. X. Chen and L. Yu, *J. Am. Chem. Soc.*, 2016, **138**, 7681–7686.
50 H. Kisch, *Angew. Chem., Int. Ed.*, 2010, **49**, 9588–9589.
51 F. Scala, *Fluidized bed technologies for near-zero emission combustion and gasification*, Woodhead Publishing, 2013.
52 R Horiba Scientific, *A guidebook to particle size analysis*, 2017.
53 Y. Pellegrin and F. Odobel, *C. R. Chim.*, 2017, **20**, 283–295.
54 R. Noriega, J. Rivnay, K. Vandewal, F. P. V. Koch, N. Stingelin, P. Smith, M. F. Toney and A. Salleo, *Nat. Mater.*, 2013, **12**, 1038–1044.
55 M. Schwarze, D. Stellmach, M. Schröder, K. Kailasam, R. Reske, A. Thomas and R. Schomäcker, *Phys. Chem. Chem. Phys.*, 2013, **15**, 3466–3472.

